

pubs.acs.org/ac Article

Divalent Metal Cation Optical Sensing Using Single-Walled Carbon Nanotube Corona Phase Molecular Recognition

Xun Gong, Soo-Yeon Cho, Sydney Kuo, Babatunde Ogunlade, Kathryn Tso, Daniel P. Salem, and Michael S. Strano*



Cite This: Anal. Chem. 2022, 94, 16393-16401



ACCESS I Metrics & More Article Recommendations Supporting Information pH 8 pH 5.7 40 Hg2+ Sensors 20 ğ **DNA-SWCNT** -60 -100 **Metal Ion Analytes**

ABSTRACT: Colloidal single-walled carbon nanotubes (SWCNTs) offer a promising platform for the nanoscale engineering of molecular recognition. Optical sensors have been recently designed through the modification of noncovalent corona phases (CPs) of SWCNTs through a phenomenon known as corona phase molecular recognition (CoPhMoRe). In CoPhMoRe constructs, DNA CPs are of great interest due to the breadth of the design space and our ability to control these molecules with sequence specificity at scale. Utilizing these constructs for metal ion sensing is a natural extension of this technology due to DNA's well-known coordination chemistry. Additionally, understanding metal ion interactions of these constructs allows for improved sensor design for use in complex aqueous environments. In this work, we study the interactions between a panel of 9 dilute divalent metal cations and 35 DNA CPs under the most controlled experimental conditions for SWCNT optical sensing to date. We found that best practices for the study of colloidal SWCNT analyte responses involve mitigating the effects of ionic strength, dilution kinetics, laser power, and analyte response kinetics. We also discover that SWCNT with DNA CPs generally offers two unique sensing states at pH 6 and 8. The combined set of sensors in this work allowed for the differentiation of Hg²⁺, Pb²⁺, Cr²⁺, and Mn²⁺. Finally, we implemented Hg²⁺ sensing in the context of portable detection within fish tissue extract, demonstrating nanomolar level detection.

INTRODUCTION

Colloidally dispersed small diameter single-walled carbon nanotubes (SWCNTs) have unique band-gap photoluminescence (PL) that absorbs photons in the visible region and emits in the near-infrared region. The photostability of this phenomenon makes these materials ideal for optical sensor applications. One common approach is the design of noncovalent nanoparticle coronas, which enable both the dispersion of these hydrophobic materials in aqueous environments as well as the control of surface features to offer selectivity toward analytes of interest.² Upon molecular adsorption of a target analyte, optical signal modulation can occur through both intensity and wavelength changes.³ This sensing scheme has been applied using a variety of corona phases (CPs) to detect multiple major classes of targets including, but not limited to, proteins, ^{4,5} reactive oxygen species, ⁶ metal ions, ⁷ steroid hormones, ⁸ and small molecules. ^{9,10} This mode of sensing is generally termed corona phase molecular recognition (CoPhMoRe). One advantage of such a system comes from the photophysical properties of the nanomaterial corona hybrid that essentially serves as both the molecular recognition and the signal transduction components of a sensor system.

One commonly studied SWCNT CP is DNA oligonucleotides, 11 where the hydrophobic nucleosides adsorb to the SWCNT surface while the negatively charged backbone forms the solution-facing component, resulting in a net negatively charged complex. The DNA CP then controls how the material interacts with its local solution environment. 12 From a sensor design point of view, this system is advantageous since

Received: August 19, 2022 Accepted: October 31, 2022 Published: November 15, 2022





the CP can be easily specified through DNA sequence design. In addition to the detection of complementary DNA, ¹³ many of the aforementioned sensors utilize this scheme. For the purposes of metal ion detection, their well-studied and sensitive biophysical coordination by DNA makes this CP choice especially promising. ¹⁴

Metal elements are present in appreciable amounts in different organ compartments of the human body. 15 Essential nutrients such as Mg, Fe, Cu, Zn, Mn, and Co are crucial in many physiological processes and must be acquired orally to avoid pathologically deficient states. 16 Conversely, certain metal elements such as arsenic, lead, mercury, and cadmium can be harmful to human health, for which levels must be closely monitored in the food and water supply, 17 especially in the case of aquaculture, where a combination of increased environmental contamination through rare-earth metal mining and biomagnification can lead to alarming concentrations of toxic metals. 18,19 While laboratory instrumentation, such as mass spectrometry, is commonly used as the gold standard for testing along the seafood supply chain, field-based rapid tests can play an important role in limiting consumer exposure in a timely manner.²

Previous literature has studied or utilized the effects of either metal particles or ions on SWCNT DNA CPs (DNA-SWCNT). Metal element nano- and microparticles have been found to assemble with colloidal SWCNTs and modulate SWCNT PL as a function of CP composition. 21,22 Fluorescently labeled DNA-SWCNTs have been used to selectively detect Ag⁺ at nanomolar concentrations.²³ Jin et al. demonstrated that ions can induce DNA-SWCNT CP conformational changes with Hg^{2+} displaying the most appreciable wavelength red shift. The quenching effect of Cu²⁺ ions on SWCNT has also been used as a part of a system to detect the presence of proteins.²⁵ Gillen et al. studied the effects of millimolar to molar concentrations of divalent metal cations on DNA-SWCNT PL, showing that metal-induced emission wavelength shifts can be mitigated using xeno nucleic acids as an alternative to DNA.26 Salem et al. showed that DNA-SWCNT PL intensity is highly dependent on a host of interdependent solution properties including ionic strength, pH, and oxygenation.²⁷ While previous work explored the significant potential of SWCNT optical sensing, the lack of explicit consistent control across these multiple solution-phase and experimental design parameters is a potential cause of variability within and between different studies, often limiting interoperability.

In this work, we develop a standardized experimental scheme for the study of SWCNT CP responses to analytes. Factors considered mitigated experimental variations from dilution, pH, and laser fluence to response kinetics. We found that a reduction of excitation fluence significantly decreases the error between technical replicates. Using these methods, a CoPhMoRe screening study was performed between a panel of DNA-SWCNTs and selected divalent metal cations at micromolar concentrations. The results show pH-dependent analyte sensitivity of SWCNT PL, with Mn²⁺, Cr²⁺, and Hg²⁺ showing the highest optical sensitivity. One of the CoPhMoRe constructs was used as part of a custom-made portable Hg²⁺ sensing setup, showing nanomolar-level detection within an extract solution from consumer market fish tissue. As a whole, while our work pertains to DNA-SWCNT and PL intensity modulation, many of our suggested best practices are readily

transferable to wavelength-responsive sensors as well as other SWCNT CoPhMoRe constructs.

EXPERIMENTAL SECTION

Materials. All chemicals were purchased from Sigma-Aldrich unless stated otherwise. ssDNA sequences were purchased from Integrated DNA Technologies (IDT). HiPco SWCNTs were used for all experiments and were purchased from Nanointegris (Batch# HR27-104). All optomechanical parts were purchased from Thorlabs (NJ) unless stated otherwise.

Preparation and Characterization of SWCNT Dispersions. SWCNT dispersions were prepared by combining 1 mg of SWCNT and 1 mg of ssDNA in 1 mL of 100 mM NaCl solution. This mixture was tip-sonicated (Qsonica Q125) in an ice bath with a 0.125 inch probe for 30 min at a power of 6-7 W. Crude SWCNT dispersions were centrifuged two times at 30,100g for 70 min to remove SWCNT bundles and other solid impurities. The top 80% of the supernatant was collected after each round of centrifugation. Absorption spectra of SWCNT dispersions were collected (Cary 5000, Agilent Technologies) to approximate the concentrations of the postdispersion stock solutions using the absorbance at 632 nm and an extinction coefficient of $\varepsilon_{632\text{nm}} = 0.036 \; (\text{mg/L})^{-1}$. cm⁻¹. Surfactant SWNT dispersions followed a similar procedure, but instead used 1 mg/mL SWCNT in a 2% (w/ v) surfactant solution dissolved in water. A final volume of 40 mL was tip-sonicated using a 6 mm probe tip (Cole Palmer) at a power of 12 W for 60 min in an ice bath. The following solution was ultracentrifuged (Beckman Coulter) using an SW32 Ti rotor at 153,000 RCF for 4 h to remove aggregates. The supernatant was collected, and absorption spectra were collected for quantification. The same extinction coefficient as above was used.

Stirred Cuvette Setup for Laser Power and Kinetic Studies. SWCNT stock solutions are diluted to a concentration of 0.5 mg/L. A 785 nm laser (450 mW B&W Tek) is connected to a 2 mm achromatic collimator (Thorlabs). The power at the sample is controlled by adding neutral density filters (Thorlabs) in the excitation beam path as well as tuning the laser output. The light then reflects off of a 900 nm longpass dichroic mirror (Thorlabs) and is focused through a 2.5 inch working distance f/3.0 noncontact objective (Kaiser Optical Systems). The light is focused into a quartz cuvette (Starna Cell) that is temperature-controlled at 25 °C through a jacket system circulating a refrigerant to control the temperature that also allows for a stir bar. The emission is collected after it passes a 900 nm long-pass filter and sent to a PI Acton SP2500 spectrometer and a Princeton Instruments InGaAs OMA V detector. For SWNT solution cuvette measurements, 2 mL of SWNT solution is added to a cuvette, and in some cases, the concentrated analyte is added to the cuvette to reach the desired final concentration. Excitation spot size in this work is calculated using the formula diameter = $1.22 \times \lambda/NA$, where λ is the excitation wavelength (785 nm), and NA, the numerical aperture of the objective (0.17). Excitation power is measured using a Thorlabs sensor (S121C).

SWCNT Near-Infrared Fluorescence Screening. SWCNT stock solutions were diluted to a concentration of 0.5 mg/L in solutions of varying pH values. These solutions were incubated at room temperature overnight to allow the systems to reach equilibrium prior to collecting fluorescence and/or absorbance measurements. Fluorescence measure-

Table 1. DNA Sequences Used for SWCNT Dispersions

K12	AGGATTCCGC	K23	GGGGGGGGGGGGGG
K13	TGGCAGCCTAAACGA	K24	CCCCCCCCC
K14	TTCAATACATACGTGACCCAGTAGTTATCC	K25	CCCCCCCCCCCC
K15	AAAAAAAA	K26	CCCCCCCCCCCCCCCCCCCCCCCCC
K16	AAAAAAAAAAAA	HM 4	CCCC GT CCCC GT CCCC GT CCCC GT CCCC
K17	AAAAAAAAAAAAAAAAAAAAAAAAAAAA	HM 5	CCCC AA CCCC AA CCCC AA CCCC AA CCCC
K18	TTTTTTTTT	HM 6	CCCC AT CCCC AT CCCC AT CCCC AT CCCC
K19	TTTTTTTTTTTTT	HM 7	CCCC TT CCCC TT CCCC TT CCCC TT CCCC
K20	TTTTTTTTTTTTTTTTTTTTTTTTTTTTTTTTT	HM 8	CCCCCC TT CCCCCC TT CCCCCC TT CCCCCC
K21	GGGGGGGG	HM 9	CCCCCC GG CCCCCC GG CCCCCC GG CCCCCC
K22	GGGGGGGGGGG		

ments were conducted in triplicate in 96-well plates (Tissue Culture Plates, Olympus Plastics) using volumes of approximately 200 µL. SWCNT solutions were excited using a 785 nm diode laser (Invictus, Kaiser Optical Systems, MI), a 20x/0.4 NA. objective LD Plan Neofluar (Zeiss, Germany), and an inverted microscope (Zeiss AxioVision). PL was collected using the same objective using the same gratings and detector as above. The exposure time held constant across was 60 s to have a significant signal-to-noise ratio. In all cases, fluorescence spectra were background-corrected using an SWCNT-free solution in an equivalent volume. During experiments in which an analyte was added, 2 µL of analyte solution (10 mM stock solutions of CdCl₂, CoCl₂, CrCl₂, CuCl₂, HgCl₂, MnCl₂, NiCl₂, PbCl₂, or ZnCl₂) was added to each well and mixed on a rocking shaker for the duration of incubation prior to collecting fluorescence measurements. Separate wells were designated as analyte-free controls.

Portable Detection and Paper Reader. Single-channel fluorescence measurements were collected using a custom-built benchtop instrument. High-powered LEDs provided sensor excitation (565 and 650 nm), and nIR fluorescence was collected using an APD photodetector with appropriate bandpass filters. Barcode strips were made using previously described methods. Briefly, a Xerox ColorQube 5780 wax printer was used to print patterns onto nitrocellulose. The paper was later baked in an oven at 105 °C for 10 min to allow the wax to melt into the porous nitrocellulose matrix. Upon cooling, SWCNT solutions were deposited onto the exposed regions of nitrocellulose as droplets and read.

Fish Tissue Extraction. Cod is purchased from a local supermarket. Two grams of tissue was ground with a hand grinder for 5 min in an extracting chemical solution of 4 mL of DI $\rm H_2O$, 5 mL of HCl (1 M), and 2 mL of $\rm o$ -nitrobenzaldehyde (10 mM) and placed in 37 °C water bath for an hour. Then, 5 mL of $\rm K_2HPO_4$ (0.1 M), 4 mL of NaOH (1 M) and 6 mL of ethyl acetate were added to the solution and centrifuged for 5 min to get the supernatant of extracted elements. For the final step, 2 mL of N-hexane and 0.5 mL of Tris-hydroxymethyl aminomethane (10 mM) was added and centrifuged for 3 min to get the final extracted solution. $\rm Hg^{2+}$ test solution is spiked with the final extracted solution and used for the barcode signal reader.

RESULTS AND DISCUSSION

SWCNT Dispersion and Measurement of Optical Responses. DNA-SWCNT dispersions are created using a common sonication and centrifugation method.²⁷ Two series of DNA sequences are chosen (Table 1). The K-series sequences are used to study the effects of length and

nucleotide composition. Specifically, we chose sequences of lengths 10, 15, and 30 by the reasoning that shorter DNA lengths would potentially result in unstable SWCNT dispersions and longer DNA lengths might be too stable and unresponsive to analytes. We studied nucleoside composition using homopolymers of each base as well as randomly generated sequences as a comparison. The HM-series sequences are designed with a majority of cytosines, interrupted by pairs of other nucleotides. Cytosines have been found to bind tightly to the SWCNT surface, which we refer to as "staple" bases. In addition, metal ion complexation in the case of double-stranded DNA often occurs through coordination between single or pairs of mismatched bases.²⁸ Thus, the HM-series offered an intuitive approach presenting spaced pairs of bases for potential adsorption sites in between islands of cytosine "staple" bases.

The optical response of SWCNTs to analytes can be measured as PL intensity changes and/or wavelength shifts. These observations are thought of as changes on or near the SWCNT surface that energetically affect the excitons generated from the band-gap PL process. One such phenomenon is solvatochromism, where the transient excited state interacts with surrounding dipoles before relaxing to the ground state, losing energy in the process. Thus, in a typical PL experiment, components that can permanently or transiently modulate SWCNT optical signals include any combination of the CP, analyte, solvent, and other solutes. In addition to standard precautions for optical measurements and performing technical replicates, the effects to control for in the case of a solution-phase DNA-SWCNT PL experiment include the following:

- Dilution and changing of ionic composition;
- buffering and choice of experimental pH;
- the effects of laser fluence;
- mitigation of SWCNT aggregation;
- response kinetic considerations.

Effects of lonic Strength and pH on Optical Response. We will first discuss the effects of solution ionic composition and pH on SWCNT PL as an interrelated phenomenon. Changes in solution ionic composition significantly affect the persistence length of the DNA molecule on the surface of the SWCNT³¹ and subsequently the surface coverage of the CP.³² Harvey et al. showed that DNA-SWCNT sensor responses against complementary strands significantly changed with solution ion type and composition.³³ Similar observations have been made for other polymer SWCNT CPs such as peptoids.³⁴

While DNA-SWCNTs are usually dispersed in NaCl solutions to promote DNA adsorption onto the SWCNT surface, sensor experiments are often performed in another

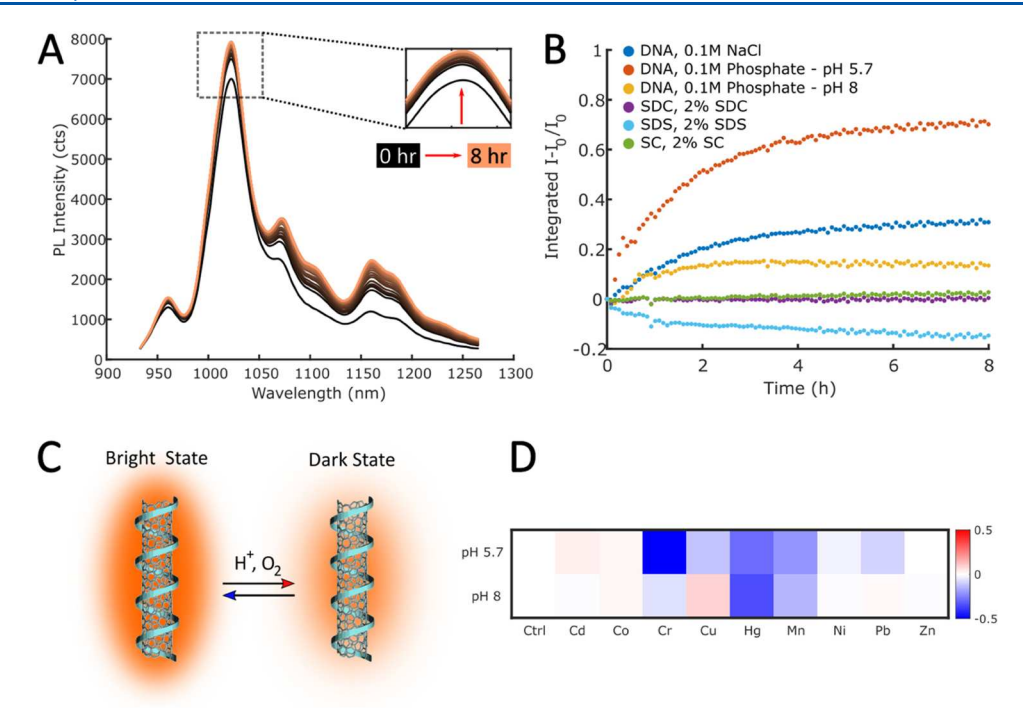


Figure 1. Solution dilution kinetics. (A) Spectral changes in the K14 DNA-SWCNT after dilution in 0.1 M phosphate buffer. (B) Integrated PL intensity change over 8 h for DNA-SWCNTs diluted in different solutions. The surfactant SWCNT dispersions in SC and SDC appear to be immune to dilution effects. (C) Schematic summarizing the effect of protons and oxygen on SWCNT PL. (D) K14 DNA-SWCNT showing significant sensor response changes, $(l-I_0)/I_0$, to 100 μ M divalent cations at pH 5.7 and pH 8 after 1 h incubation.

buffer. To investigate sensing experimental conditions in detail, we chose a randomly generated length 30 DNA CP (sample K14). Figure 1A shows repeated PL emission spectra taken on K14 DNA-SWCNTs diluted from NaCl into a sodium phosphate buffer (pH 5.7, 0.1 M) over the course of 8 hr. The observed increased PL affected all SWCNT chiralities present in the sample. To quantify the optical signal change, we calculated an integrated PL intensity over the measured wavelength range using the parameter $(I-I_0)/I_0$, where I is the integrated PL intensity (850–1250 nm) at a time of interest and I_0 is the integrated PL intensity at the start of the experiment. As this study was performed using a single 785 nm excitation, we decided to report normalized integrated intensities only because fitting to 12 SWCNT species would introduce significant inaccuracies.

Figure 1B shows the kinetics of optical response changes of DNA-SWCNT diluted into several different buffer conditions. As a comparison, surfactant-dispersed SWCNTs are diluted into their respective dispersion solvents. Sodium cholate (SC) and sodium deoxycholate (SDC) CPs are immune to these dilution effects while the sodium dodecyl sulfate (SDS) sample was not. The kinetics of the dilution effect occurred over hours and are likely attributable to the slow reorganization of the fluid CP, following a change in the local environment. For the purposes of experimental control in solution-phase sensing experiments, we recommend sample dilution in the buffer of choice for a minimum of 6 h.

The relationship between protons, or pH, and colloidal SWCNT PL is more complex. In the case of SC-SWCNTs, the observed spectral shifts with pH change were attributed to the protonation of the corona molecules.³⁶ In DNA-SWCNTs, Nißler et al. showed that pH can modulate SWCNT PL intensity in a sequence-dependent manner.³⁷ In experiments of aqueous two-phase separation of DNA-SWCNTs, solution-

phase pH significantly altered the partitioned population and yield of the method. 38

In 2017, we reported the relationship between ionic strength, pH, O_2 , and DNA-SWCNT PL.²⁷ Briefly, the DNA CP converts between two phases driven by solution ionic strength. Each phase is affected differently by H⁺-induced, reversible optical transition bleaching, for which dissolved O_2 is a required component. In other words, H⁺ and O_2 are two outside factors to control for in the case of a dilution-equilibrated PL study (Figure 1C). Considering that laboratory O_2 levels are consistent, and that samples are mixed in a similar manner, then solution pH would be a main factor for control.

In addition to the H⁺ effect as a part of the two-phase model, we also need to consider the effect of CP protonation on its structure as highlighted in the case of SC. For nucleic acids, complex folded states can be modulated by protonation and deprotonation, ³⁹ especially in short sequences where the pK_a can be between pH 6 and 8.40 While the exact sequencedependent structure of the DNA-SWCNT CP is unclear, protonation undoubtedly results in significant changes. Thus, we propose that low and high pH states should be regarded as separate sensing constructs. For this study, we choose phosphate buffer, which spans the pH range interest to create two sensing conditions at pH 5.7 and 8. Figure 1D shows the K14 CP optical response at the two specified pH states against a panel of divalent metal ions at 100 μM with 1 h incubation. Optical response in Figure 1 is calculated as $(I - I_0)/I_0$, where I_0 is the integrated PL spectral intensity prior to analyte incubation and I is the value after analyte incubation. The significant and differential optical responses between the two pH conditions support the above determination.

Control of Laser Fluence. One experimental parameter often not explicitly addressed in SWCNT optical sensor studies is the effect of sample exposure to differences in

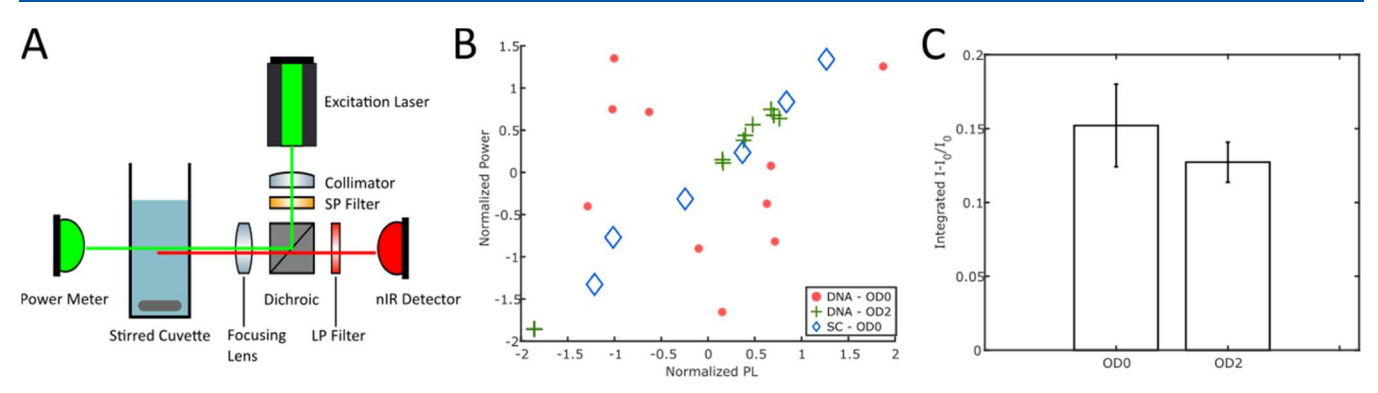


Figure 2. Influence of excitation fluence. (A) Schematic of the stirred cuvette setup to concurrently measure excitation power and emission PL. (B) Normalized fluence versus normalized PL plot. Low laser fluence stepping of DNA-SWCNT shows a linear trend similar to SC-SWCNT, while high laser fluence DNA-SWCNT shows significant variability. Based on hardware specifications and measured values, accuracy of the reported excitation power and emission PL is <1 and <5%, respectively. (C) Comparing multiple replicates of DNA-SWCNT response to 100 μ M Hg²⁺, OD2 measurements show decreased variability (error bars are standard deviation).

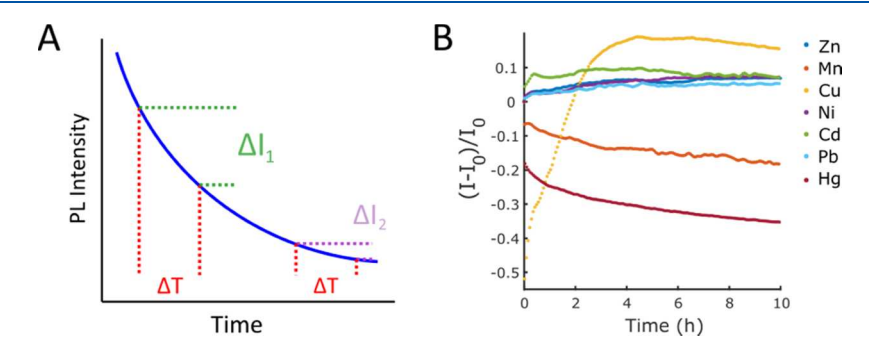


Figure 3. Effect of measurement time. (A) Diagram showing PL response kinetics over time and how measurement error can arise from sample incubation time and (B) 100 μ M cation responses of K14 DNA-SWCNT at pH 5.7 show slow kinetics on the order of hours and a unique signal recovery of Cu²⁺.

excitation power. While the excitation hardware is listed in previous work, differences in optomechanical components and device alignment will influence the power received by the sample. To study this effect, a custom-made setup was constructed consisting of a light source focused onto a stirred quartz cuvette with a visible detector to measure excitation power through the cuvette and a nIR detector for SWCNT PL across a dichroic (Figure 2A). We define laser fluence as the average power at a Gaussian beam waist in mW/cm². Laser power levels were stepped downward at 5% intervals while allowing sufficient time for PL to equilibrate (Figure S1). Using an OD2 neutral density filter on the excitation path, a "low fluence" experimental condition was created. The signalto-noise ratio was maintained by increasing the integration time for the OD2 case. The starting fluences of the OD0 (high power) and OD2 (low power) conditions were 6.44×10^5 and 1.78×10^4 mW/cm², respectively.

Here, we use K14, the random 30-mer DNA CP, to test the effects of excitation fluence. In the stepping experiment, an ideal fluorophore emission is expected to linearly decrease with the 5% decreasing steps. To directly compare the point spread of the experimental conditions that have different absolute ranges in both axes, we have performed the following normalization: $X_{\text{norm}} = (X - X_{\mu})/X_{\sigma}$, where X is an array of data PL or laser power, X_{μ} the average of X, and X_{σ} the standard deviation of X (Figure 2B). Results show that both SC-SWCNT at OD0 and DNA-SWCNT at OD2 observe a linear relationship ($R^2 = 0.996$ and $R^2 = 0.98$, respectively) while DNA-SWCNT at OD0 does not ($R^2 = 0.01$). In other

words, high laser fluence has a significant effect on DNA-SWCNT PL. To evaluate the effects of this observed variability on sensor responses, DNA-SWCNT response to Hg^{2+} was measured multiple times in this stirred setup. The "low fluence" state experiment showed a decreased standard deviation between replicates (Figure 2C). Thus, we recommend SWCNT optical studies to be performed at low laser fluence on the order of 2×10^4 mW/cm² measured at the sample to decrease measurement variability. Further decreases of excitation power might be beneficial but will come at the cost of integration time, signal-to-noise ratio, and temporal resolution.

Aggregation and Optical Response Kinetics, Another significant source of experimental variability is the solutionphase aggregation of SWCNTs. This phenomenon is frequently observed with surfactant SWCNTs, including salt addition in SDS-SWCNT⁴¹ and metal ion complexation of SDBS-SWCNT.⁴² DNA-SWCNT can also form loose associations that can affect optical properties.⁴³ Colloidal aggregation behavior is known to be stochastic, difficult to model, and can present challenges for experimental replication.44 From Koh et al.'s study, detailing the effects of SWCNT aggregation as a function of ionic composition and concentration, DNA-SWCNTs appear to be stable at 100 mM salt concentrations, a value we choose to maximally retain buffering capacity. 45 Another consideration is SWCNT concentration, which can be lowered to decrease collision events. We choose 0.5 mg/L to be most dilute while maintaining reasonable experimental integration times.

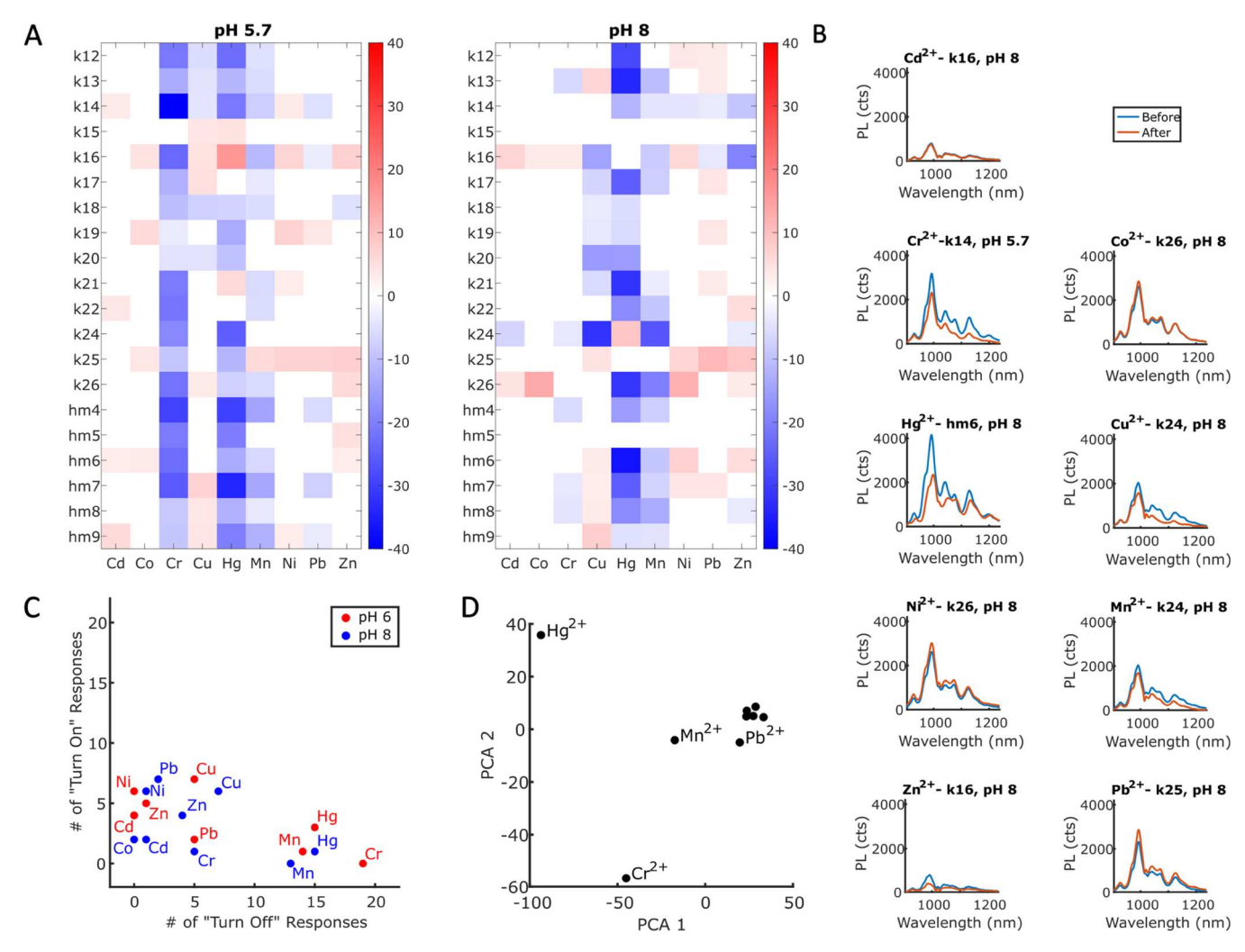


Figure 4. Sensor screen results. (A) Sensor responses with Z > 3 (two-tailed, P < 0.0027) for the panel of DNA-SWCNTs versus cations across two different reaction pH values. (B) Spectral changes of highest responders for each cation species. (C) Plot showing the total "turn on" versus "turn off" responses for each experimental condition. (D) Combined PCA analysis of all sequences and pH conditions, showing differentiability for Hg^{2+} , Cr^{2+} , Mn^{2+} , and Pb^{2+} .

Given that SWCNT optical responses often involve adsorption to and rearrangement of surface CPs, it is unsurprising that the kinetics of these responses are on the order of minutes to hours. For example, the time constant for a SC-induced PL shift in a 12 base-pair DNA CP is about 2 h. 46 Similarly, metal ions are known to interact with DNA, many of which do so on the order of hours.⁴⁷ The disadvantages of taking an early measurement given slower kinetics include (1) a decrease of potential signal-to-noise ratio and (2) an increase in method error between replicates due to experimental timing. Figure 3A shows a typical optical response that equilibrates over time. Assuming that the timing of each incubation has an error of ΔT , then measuring at early times will have a larger error in PL intensity. Thus, knowing the kinetics of the response is an important factor to consider. Figure 3B shows the response kinetics of sample K14 to our panel of analytes at pH 5.7. Significant responses included Mn²⁺, Hg²⁺, and Cu²⁺. Surprisingly, while Cu2+ is known to cause significant quenching in DNA-SWCNT, signal recovery over the course of 4 h was not previously observed. Finally, since SWCNT sensors are often considered as candidates for field-based rapid tests, measuring at exceedingly long incubations is not practical. In this study, we found a standard 1 h incubation

to be reasonably consistent. A comparison of 1 hr versus 2 h incubation for a set of DNA-SWCNTs against Mn^{2+} is shown in Figure S2.

Divalent Metal Cations Results. Based on the above explicit control experiments, a sensor response screen was performed between a panel of DNA-SWCNTs and our divalent metal ions of interest at 100 μ M concentrations. Specifically, Cd, Hg, Pb, Ni, and Cr are chosen due to their presence as the most common toxic trace metals in aquaculture. Since each study is performed in three technical replicates, we choose two-tailed Z-values to represent statistically significant optical responses between integrated intensities of metal ion and control groups. Figure 4A displays screen results of each analyte/sensor combination with Z > 3 (two-tailed, P < 0.0027). This metric was also used to classify a response as "turn on" or "turn off". Mean integrated intensity results are shown in Figure S3.

Comparing the two pH conditions, optical responses changed sign 39% (71/180) of the time. Of note, Cr²⁺ had a significant negative response across all sequences at pH 6, which was decreased at pH 8. For each metal ion species, the largest responders and their spectral changes are shown in Figure 4B. The most significant responses include Cu²⁺, Cr²⁺,

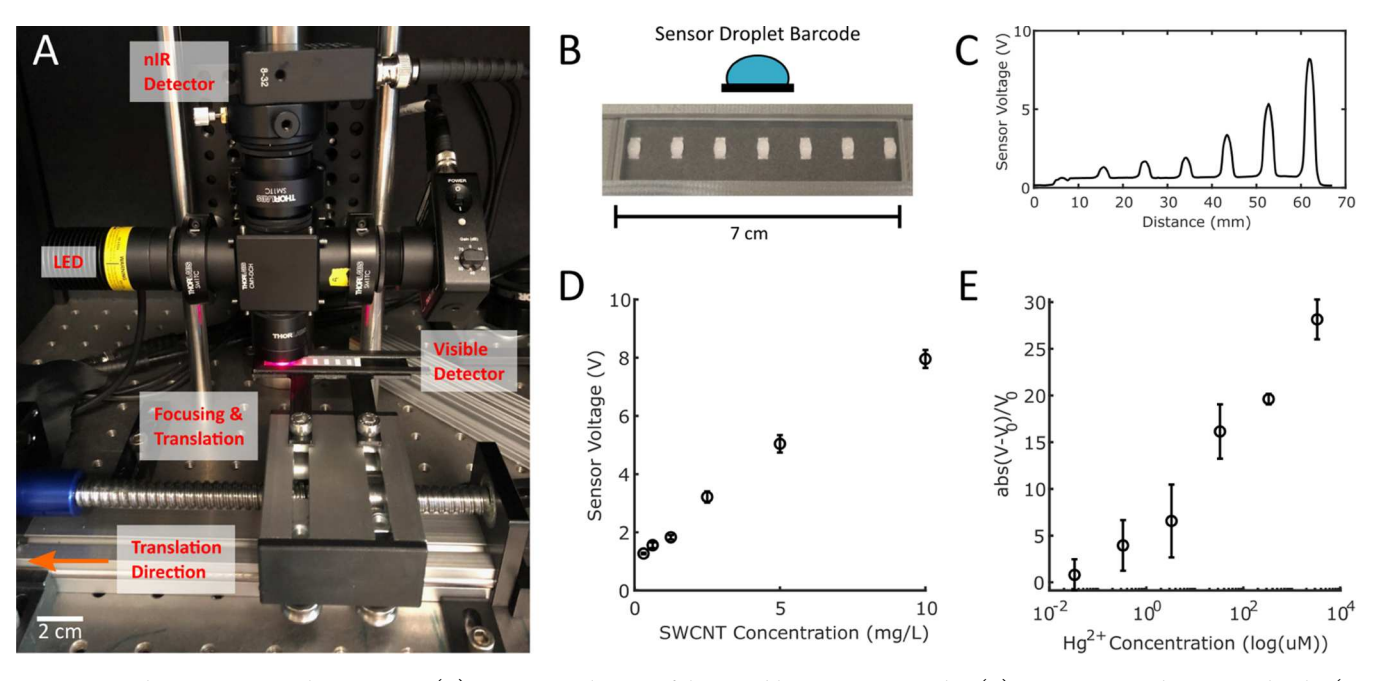


Figure 5. Application in aquaculture sensing. (A) Experimental setup of the portable sensor strip reader. (B) Sensor strip and SWCNT droplet (0, 0.3125, 0.625, 1.25, 2.5, 5, and 10 mg/L from left to right droplet) geometry for the signal reading. (C) Real-time signal output of barcode moving from right to left. (D) Detection of SWCNT PL at different solution SWCNT concentrations to determine the signal-to-noise ratio of the system. (E) Hg²⁺ sensing response of the highest-performing DNA-SWCNT. The limit of detection is down to 33 nM.

Hg²⁺, and Mn²⁺. Of this group, Hg²⁺ showed the most significant wavelength shift in addition to intensity change. The nucleotide base thymine along with AT-rich sequences have been previously found to bind to Hg²⁺.⁴⁹ We found that CPs HM6 and HM7 had the strongest optical responses, and they consist of "staple" cytosines interspaced with AT and TT regions, respectively. Additionally, other than Cr²⁺, other best sensor candidates are from the pH 8 group. To further analyze the differences in "turn on" versus "turn off" responses for each metal ion and pH condition, the number of each type of response is plotted in Figure 4C. There are two groups: one with equally low number of each type of response and the other with strong "turn off" responses across all sequences. Cr2+ is the most unique due to the differences in pH conditions. We hypothesize that the Cr²⁺ interaction is likely more with the DNA, as the protonated strands at pH 8 offer less ability for metal ion coordination. Though Cu²⁺ shows mild responses, possibly due to signal recovery kinetic seen earlier, sample K24 at pH 8 showed a strong "turn off" response, suggesting that Cu²⁺ may interact more directly with the SWCNT surface. Examining the three lengths of each homogeneous CP, samples K15-26, it was unclear that PL responses have a length dependence. To aggregate these results and look for general trends, magnitude of each response regardless of nucleoside identity was plotted against CP (Figure S4). No length dependence was observed in this combined analysis, suggesting that PL responses to these ions are either specific CP structure-dependent or modulated by longer-length DNA CPs. Finally, we performed principal component analysis (PCA) for the entire data set, treating each DNA-SWCNT and pH combination as independent observations. Given the available sensor set and assuming the independence of features, we are able to show differentiability for Hg²⁺, Cr²⁺, Mn²⁺, and Pb²⁺ using the first two significant components (Figure 4D). Interestingly, Pb²⁺ is not as

differentiable when performing PCA on each pH individually (Figures S5 and S6).

Hg²⁺ Sensing for Aquaculture Applications. As a more realistic test solution phase sensing, we implemented the HM6 DNA-SWCNT for Hg²⁺ as part of a portable system for sensing in aquaculture applications. A previously described custom-made miniature optical setup is used to simulate field application hardware including LED excitation, an avalanche photodiode detector for nIR detection, a visible sensor for excitation correction, and a translational stage for sample reading (Figure 5A).²⁰ Low-cost rapid test devices usually consist of single-channel detectors and maximize the signal-tonoise ratio by measuring total signal over a wavelength range. Thus, the integrated PL results should translate directly into our prototype.

To prepare the sensors, they were drop-cast on the printed barcode with hydrophobic (gray regions) wells (Figure 5B). After allowing DNA-SWCNT to enter the paper matrix, any excess was removed *via* washing. For each sensing experiment, the analyte sample was then loaded as droplets above the regions containing the SWCNT, each well being a separate experimental condition. By translating the barcode across a focused lens, a readout of peaks representing the SWCNT signal is produced (Figure 5C). Figure 5D shows a calibration curve showing that DNA-SWCNT is detected down to $\mu g/mL$ -level concentrations (0.3125 $\mu g/mL$).

To simulate the detection of Hg^{2+} from consumer market fish tissue, we create a test solution using supermarket-purchased cod and a standard extraction protocol used by commercially available rapid tests for small molecules. Fish tissue was ground and incubated with HCl and 2-nitrobenzaldehyde at 60 °C for 1 hr (detailed extraction process in the experimental section). The sample was then centrifuged and cleaned with ethyl acetate and then hexane. The aqueous phase was then used as a spike solution for our Hg^{2+} detection. Using the portable reader and the droplet barcode method, we

were able to detect 33 nM Hg²⁺ in the test solvent (Figure 5E). Considering that the average mercury concentration in cod is 0.11 ppm^{50} or $1.1 \mu\text{M}$ following extraction, this technology should be applicable for commercial applications.

CONCLUSIONS

In this work, we study the effect of dilute divalent metal cations on DNA-SWCNTs for the purposes of CoPhMoRe sensor development. First, we optimize for factors to control for in solution-phase SWCNT/analyte photophysical studies. We found that the most reproducible experiments involved controlling for buffer dilution kinetics, solution pH, SWCNT aggregation, excitation power, and measurement relative to response kinetics. Especially for optical setups using lasers of hundreds of milliwatts, measuring and decreasing sample exposure is critical. Additionally, since pH affects both the CP and the SWCNT itself, it makes sense to define the SWCNT dispersion at large pH differences as potentially separate sensing constructs. To summarize, we recommend the following conditions for a DNA-SWCNT solution-phase sensing experiment: (1) dilution overnight in the test buffer of choice, (2) choosing different pH 6 and 8 as separate experimental conditions, (3) limit excitation fluence to the order of 2×10^4 mW/cm², (4) SWCNT concentration of 0.5 mg/L and an ionic concentration of 100 mM to minimize aggregation, and (5) analyte response incubation time commensurate with observed kinetics. Using these methods, we studied the response of a panel of DNA-SWCNTs against the metal ions of interest at dilute concentrations. We found significant pH-dependent response differences, supporting the hypothesis that sufficiently different pH states of the sample CP can perform as separate sensing constructs, contributing orthogonal information. Combining the sensor and experimental conditions explored, we were able to differentiate Hg²⁺, Cr²⁺, Mn²⁺, and Pb²⁺. Finally, we implemented a Hg²⁺ responding sensor candidate in the setting of a portable reader for aquaculture applications. Calibration in fish extract solution shows that the detection limit of the current system is in the nanomolar range.

It is important to note that this work used HiPco SWCNT samples consisting of 12 SWCNT chirality species, each of which contributes linearly to the total integrated signal. From a broadband portable detector point of view, changes in the chirality distribution could result in different calibration curves and signal-to-noise ratio, due to normalization. Recently, these concerns are minimal due to consistent chirality distributions in SWCNT manufacturing. More importantly, this work detailed the effect of dilute metal ions on DNA-SWCNTs as a function of solution conditions and pH-dependent sensing. The experimental controls developed here are valuable considerations for the field to both improve data quality and reproducibility.

ASSOCIATED CONTENT

Supporting Information

The Supporting Information is available free of charge at https://pubs.acs.org/doi/10.1021/acs.analchem.2c03648.

Supporting information contains example readings from excitation power stepping experiments; additional sensor responses against 100 uM Mn; results from Figure 4 displayed as $(I - I_0)/$; analysis of DNA sequence length

versus PL response; and separate PCA analysis of sensors at pH 5.7 and 8 (Figure S5) (PDF)

AUTHOR INFORMATION

Corresponding Author

Michael S. Strano — Department of Chemical Engineering, Massachusetts Institute of Technology, Cambridge, Massachusetts 02139, United States; orcid.org/0000-0003-2944-808X; Email: strano@mit.edu

Authors

Xun Gong — Department of Chemical Engineering, Massachusetts Institute of Technology, Cambridge, Massachusetts 02139, United States; orcid.org/0000-0003-4168-2768

Soo-Yeon Cho — School of Chemical Engineering, Sungkyunkwan University, Suwon 16419, Republic of Korea; oorcid.org/0000-0001-6294-1154

Sydney Kuo – Department of Chemical Engineering, Massachusetts Institute of Technology, Cambridge, Massachusetts 02139, United States

Babatunde Ogunlade – Department of Chemical Engineering, Massachusetts Institute of Technology, Cambridge, Massachusetts 02139, United States

Kathryn Tso — Department of Chemical Engineering, Massachusetts Institute of Technology, Cambridge, Massachusetts 02139, United States

Daniel P. Salem – Department of Chemical Engineering, Massachusetts Institute of Technology, Cambridge, Massachusetts 02139, United States

Complete contact information is available at: https://pubs.acs.org/10.1021/acs.analchem.2c03648

Author Contributions

X.G. contributed to all aspects of the work. S.-Y.C. performed the fish tissue measurement study. S.K., B.O., and K.T. aided in sensor microscopy and screening experiments. D.P.S. helped conceive ideas. M.S.S. mentored the project and reviewed the publication. All authors have given approval to the final version of the manuscript.

Notes

The authors declare no competing financial interest.

ACKNOWLEDGMENTS

The research was partially supported by an award from the Walmart Foundation and the Walmart Food Safety Collaboration Center in Beijing. This research was partially supported by the NSF Biosensing Program under award number 2124194. This work was supported as part of the funding from the Disruptive & Sustainable Technology for Agricultural Precision (DiSTAP) of the Singapore MIT Alliance for Research and Technology (SMART) Center.

ABBREVIATIONS

SWCNT single-walled carbon nanotube

DNA deoxyribonucleic acid SC sodium cholate SDC sodium deoxycholate SDS sodium dodecyl sulfate

REFERENCES

- (1) O'Connell, M. J.; Bachilo, S. M.; Huffman, C. B.; Moore, V. C.; Strano, M. S.; Haroz, E. H.; Rialon, K. L.; Boul, P. J.; Noon, W. H.; Kittrell, C.; Ma, J.; Hauge, R. H.; Weisman, R. B.; Smalley, R. E. Science 2002, 297, 593–596.
- (2) Zhang, J.; Landry, M. P.; Barone, P. W.; Kim, J.-H.; Lin, S.; Ulissi, Z. W.; Lin, D.; Mu, B.; Boghossian, A. A.; Hilmer, A. J.; Rwei, A.; Hinckley, A. C.; Kruss, S.; Shandell, M. A.; Nair, N.; Blake, S.; Şen, F.; Şen, S.; Croy, R. G.; Li, D.; Yum, K.; Ahn, J.-H.; Jin, H.; Heller, D. A.; Essigmann, J. M.; Blankschtein, D.; Strano, M. S. *Nat. Nanotechnol.* 2013, 8, 959–968.
- (3) Landry, M. P.; Kruss, S.; Nelson, J. T.; Bisker, G.; Iverson, N. M.; Reuel, N. F.; Strano, M. S. Sensors 2014, 14, 16196–16211.
- (4) Bisker, G.; Bakh, N. A.; Lee, M. A.; Ahn, J.; Park, M.; O'Connell, E. B.; Iverson, N. M.; Strano, M. S. ACS Sens. 2018, 3, 367–377.
- (5) Salem, D. P.; Gong, X.; Lee, H.; Zeng, A.; Xue, G.; Schacherl, J.; Gibson, S.; Strano, M. S. ACS Sens. 2020, 5, 327-337.
- (6) Ulissi, Z. W.; Sen, F.; Gong, X.; Sen, S.; Iverson, N.; Boghossian, A. A.; Godoy, L. C.; Wogan, G. N.; Mukhopadhyay, D.; Strano, M. S. *Nano Lett.* **2014**, *14*, 4887–4894.
- (7) Lew, T. T. S.; Park, M.; Cui, J.; Strano, M. S. Adv. Mater. 2021, 33, No. 2005683.
- (8) Lee, M. A.; Wang, S.; Jin, X.; Bakh, N. A.; Nguyen, F. T.; Dong, J.; Silmore, K. S.; Gong, X.; Pham, C.; Jones, K. K.; Muthupalani, S.; Bisker, G.; Son, M.; Strano, M. S. Adv. Healthcare Mater. 2020, 9, No. e2000429.
- (9) Bhattacharya, S.; Gong, X.; Wang, E.; Dutta, S. K.; Caplette, J. R.; Son, M.; Nguyen, F. T.; Strano, M. S.; Mukhopadhyay, D. *Cancer Res.* **2019**, *79*, 4515–4523.
- (10) Kozawa, D.; Cho, S.-Y.; Gong, X.; Nguyen, F. T.; Jin, X.; Lee, M. A.; Lee, H.; Zeng, A.; Xue, G.; Schacherl, J.; Gibson, S.; Vega, L.; Strano, M. S. ACS Nano 2020, 14, 10141–10152.
- (11) Zheng, M.; Jagota, A.; Strano, M. S.; Santos, A. P.; Barone, P.; Chou, S. G.; Diner, B. A.; Dresselhaus, M. S.; McLean, R. S.; Onoa, G. B.; Samsonidze, G. G.; Semke, E. D.; Usrey, M.; Walls, D. J. *Science* **2003**, 302, 1545–1548.
- (12) Griffith, D. M.; Jayaram, D. T.; Spencer, D. M.; Pisetsky, D. S.; Payne, C. K. *Biointerphases* **2020**, *15*, No. 051006.
- (13) Heller, D. A.; Jeng, E.; Yeung, T.; Martinez, B.; Moll, A.; Gastala, J.; Strano, M. Science **2006**, 311, 508–511.
- (14) Zhou, W.; Saran, R.; Liu, J. Chem. Rev. 2017, 117, 8272-8325.
- (15) Zaksas, N. P.; Soboleva, S. E.; Nevinsky, G. A.. Twenty Element Concentrations in Human Organs Determined by Two-Jet Plasma Atomic Emission Spectrometry *Sci. World J.*, **2019**, 2019, 1–9, https://www.hindawi.com/journals/tswj/2019/9782635/, DOI: 10.1155/2019/9782635.
- (16) Lakatos, B.; Szentmihályi, K.; Vinkler, P.; Balla, J.; Balla, G. *Orv Hetil* **2004**, *145*, 1315–1319.
- (17) US Food and Drug Administration. *Metals and Your Food*; FDA https://www.fda.gov/food/chemicals-metals-pesticides-food/metals-and-your-food (accessed February 28, 2021).
- (18) Jara-Marini, M. E.; Molina-García, A.; Martínez-Durazo, Á.; Páez-Osuna, F. *Environ. Sci. Pollut. Res. Int.* **2020**, 27, 5323–5336.
- (19) Jin, C.; Levi, R.; Liang, Q.; Renegar, N.; Springs, S.; Zhou, J.; Zhou, W. Manage. Sci. 2021, 67, 2985–2996.
- (20) Salem, D. P.; Gong, X.; Liu, A. T.; Akombi, K.; Strano, M. S. Anal. Chem. **2020**, 92, 916–923.
- (21) Wang, D.; Li, Z.-C.; Chen, L. J. Am. Chem. Soc. 2006, 128, 15078-15079.
- (22) Kim, S.-J.; Park, J.; Jeong, Y.; Go, H.; Lee, K.; Hong, S.; Seong, M.-J. Nanoscale Res. Lett. **2014**, 9, No. 85.
- (23) Zhao, C.; Qu, K.; Song, Y.; Xu, C.; Ren, J.; Qu, X. Chem. Eur. J. 2010, 16, 8147-8154.
- (24) Jin, H.; Jeng, E. S.; Heller, D. A.; Jena, P. V.; Kirmse, R.; Langowski, J.; Strano, M. S. *Macromolecules* **2007**, *40*, 6731–6739.
- (25) Nelson, J. T.; Kim, S.; Reuel, N. F.; Salem, D. P.; Bisker, G.; Landry, M. P.; Kruss, S.; Barone, P. W.; Kwak, S.; Strano, M. S. *Anal. Chem.* **2015**, *87*, 8186–8193.

- (26) Gillen, A. J.; Kupis-Rozmysłowicz, J.; Gigli, C.; Schuergers, N.; Boghossian, A. A. J. Phys. Chem. Lett. 2018, 9, 4336–4343.
- (27) Salem, D. P.; Gong, X.; Liu, A. T.; Koman, V. B.; Dong, J.; Strano, M. S. J. Am. Chem. Soc. 2017, 139, 16791–16802.
- (28) Gao, J.; Berden, G.; Rodgers, M. T.; Oomens, J. Phys. Chem. Chem. Phys. **2016**, 18, 7269–7277.
- (29) Zhou, W.; Ding, J.; Liu, J. Biosens. Bioelectron. 2017, 87, 171–177.
- (30) Kasprowicz, A.; Stokowa-Sołtys, K.; Wrzesiński, J.; Jeżowska-Bojczuk, M.; Ciesiołka, J. *Dalton Trans.* **2015**, *44*, 8138–8149.
- (31) Li, Z.; Song, Y.; Li, A.; Xu, W.; Zhang, W. Nanoscale 2018, 10, 18586-18596.
- (32) Park, M.; Salem, D. P.; Parviz, D.; Gong, X.; Silmore, K. S.; Lew, T. T. S.; Khong, D. T.; Ang, M. C.-Y.; Kwak, S.-Y.; Chan-Park, M. B.; Strano, M. S. *Nano Lett.* **2019**, *19*, 7712–7724.
- (33) Harvey, J. D.; Zerze, G. H.; Tully, K. M.; Mittal, J.; Heller, D. A. J. Phys. Chem. C **2018**, 122, 10592–10599.
- (34) Chio, L.; Del Bonis-O'Donnell, J. T.; Kline, M. A.; Kim, J. H.; McFarlane, I. R.; Zuckermann, R. N.; Landry, M. P. *Nano Lett.* **2019**, 19, 7563–7572.
- (35) Rocha, J.-D. R.; Bachilo, S. M.; Ghosh, S.; Arepalli, S.; Weisman, R. B. *Anal. Chem.* **2011**, *83*, 7431–7437.
- (36) Li, H.; Zhou, L.; Smolinski, N. K. J. Phys. Chem. C 2019, 123, 2565–2572.
- (37) Nißler, R.; Mann, F. A.; Chaturvedi, P.; Horlebein, J.; Meyer, D.; Vuković, L.; Kruss, S. J. Phys. Chem. C 2019, 123, 4837–4847.
- (38) Lyu, M.; Meany, B.; Yang, J.; Li, Y.; Zheng, M. J. Am. Chem. Soc. 2019, 141, 20177-20186.
- (39) Thaplyal, P.; Bevilacqua, P. C. Methods Enzymol. 2014, 549, 189-219.
- (40) Siegfried, N. A.; O'Hare, B.; Bevilacqua, P. C. Biochemistry 2010, 49, 3225-3236.
- (41) Niyogi, S.; Boukhalfa, S.; Chikkannanavar, S. B.; McDonald, T. J.; Heben, M. J.; Doorn, S. K. J. Am. Chem. Soc. 2007, 129, 1898–1800
- (42) Brege, J. J.; Gallaway, C.; Barron, A. R. J. Phys. Chem. C 2007, 111, 17812-17820.
- (43) Gong, X.; Sharma, A. K.; Strano, M. S.; Mukhopadhyay, D. ACS Nano 2014, 8, 9126–9136.
- (44) Shen, J.-L.; Tsai, M.-Y.; Schafer, N. P.; Wolynes, P. G. J. Phys. Chem. B 2021, 125, 1118–1133.
- (45) Koh, B.; Cheng, W. Langmuir 2014, 30, 10899-10909.
- (46) Alizadehmojarad, A. A.; Zhou, X.; Beyene, A. G.; Chacon, K. E.; Sung, Y.; Pinals, R. L.; Landry, M. P.; Vuković, L. Adv. Mater. Interfaces 2020, 7, No. 2000353.
- (47) Li, W.; Zhang, Z.; Zhou, W.; Liu, J. ACS Sens. 2017, 2, 663-
- (48) Shorna, S.; Shawkat, S.; Hossain, A.; Quraishi, S. B.; Ullah, A. K. M. A.; Hosen, M. M.; Hossain, M. K.; Saha, B.; Paul, B.; Habibullah-Al-Mamun, M. *Biol. Trace Elem. Res.* **2020**, DOI: 10.1007/s12011-020-02450-y.
- (49) Nehzati, S.; Summers, A. O.; Dolgova, N. V.; Zhu, J.; Sokaras, D.; Kroll, T.; Pickering, I. J.; George, G. N. *Inorg. Chem.* **2021**, *60*, 7442–7452.
- (50) US Food & Drug Administration. Technical Information on Development of FDA/EPA Advice about Eating Fish for Those Who Might Become or Are Pregnant or Breastfeeding and Children Ages 1-11 Years; FDA, 2022.